A weighted distributed predictor-feedback control synthesis for interconnected time delay systems[☆]

Antonio González

Abstract

The paper investigates the control design of interconnected time delay systems by means of distributed predictor-feedback delay compensation approaches and event-triggered mechanism. The idea behind delay compensation is to counteract the negative effects of delays in the control-loop by feeding back future predictions of the system state. Nevertheless, an exact prediction of the overall system state vector cannot be obtained providing that each system has only knowledge of their local data regarding the system model and state variables. Consequently, predictor-feedback delay compensation may lose effectiveness if the coupling between subsystems is sufficiently strong. To circumvent this drawback, the proposed distributed predictor-feedback control incorporates extra degree of freedom for control synthesis by introducing new weighting factors for each local prediction term. The design of the weighting factors is addressed, together with the event-triggered parameters, by an algorithm based on Linear Matrix Inequalities (LMI) and the Cone Complementarity Linearization (CCL). Simulation results are provided to show the achieved improvements and validate the effectiveness of the proposed method, even in the case that other control strategies fail to stabilize the closed-loop system.

Keywords: Delay compensation, Distributed control, Interconnected system, Time delay, Event-triggered Control, Linear Matrix Inequality (LMI)

[☆]a) This manuscript is the authors' original work and has not been published nor has it been submitted simultaneously elsewhere. b) All authors have checked the manuscript and have agreed to the submission. The corresponding author is A. Gonzalez. He is with the Instituto de Automática e Informática Industrial (AI2), Universitat Politècnica de València (UPV), Spain. (e-mail: angonsor@upv.es).

1. Introduction

Time delays are inevitably encountered in a great variety of engineering applications, such as networked control systems [1, 2, 3, 4, 5] and multiagent systems [6, 7, 8, 9]. The presence of delays may cause instability or poor performance in the control system if they are not taken into account in the control design stage [10]. This fact has motivated over the last decades the research of advanced control strategies to compensate the negative effects of delays in the closed-loop dynamics (see [11, 12, 13] and references therein). Most of these methods are extensions of the classical Smith Predictor [14], and the Finite Spectrum Assignment or predictor-feedback control [15]. Smith predictor control uses prior knowledge of the plant model to remove the delayed dynamics of the control system by internal model control. Predictor-feedback control allows obtaining an equivalent delay-free closed-loop system by applying a state transformation based on the Artstein's reduction method [16]. The underlying idea behind delay compensation is to anticipate the system behavior in the control loop by predicting the state variable. Thus, any controller designed to stabilize the delay-free control system can ensure the stability for arbitrarily large delays, provided that an exact description of the plant model and time delays is available for state prediction. In the presence of model uncertainties and delay mismatches, further studies revealed that better robust performance can be achieved by predictor-feedback delay compensation under different implementations: discrete-time predictor feedback [17, 18, 19], event-triggered predictor feedback [20], truncated predictor-feedback [21], nonlinear predictor feedback in continuous-time [22, 23, 13] and discrete-time [24]. Nevertheless, most of these studies are focused on centralized controllers and, to the best author's knowledge, few works investigate the stabilization of interconnected time systems under delay compensation approaches.

Interconnected systems consist of multiple coupled subsystems provided with local controllers independent of the others, where each controller can only access the past and current information of the corresponding subsystem. Hence, a distributed control architecture is appropriate for interconnected systems, such as multiagent systems or complex systems with strong interactions [25]. For interconnected time delay systems, observer-predictor delay compensation methods were proposed in [26, 27] to address the output consensus design of networked multiagent systems. A delay compensation based on multiple Smith predictors was further proposed in [28] to solve the

formation control synthesis of multiagent systems. Nevertheless, the following drawbacks still hold: (i) each agent requires full knowledge of the overall interconnected system model, and (ii) the complexity of each local controller is proportional to the number of systems. Other related delay compensation strategies were proposed for consensus of multiagent systems by truncated predictor-feedback approaches [29, 30, 31], discrete-time predictor-feedback consensus [32, 33, 34]. A predictor-feedback control was also proposed to stabilize two interconnected time delay systems based on a PDE representation of delayed input [35]. In contrast to previous approaches, the complexity of each local controller in [35] is independent of the number of subsystems and only local data regarding the system model and state variables is required for each controller. Nevertheless, a state prediction without error cannot be obtained and delay compensation might therefore lose effectiveness if the coupling between systems is enough strong.

In this paper, a novel distributed predictor-feedback control is proposed by introducing weighting factors for each local predictor-feedback term. The key idea is to reduce the negative effect of prediction error in the control system by suitably designing such weighting factors. Moreover, we consider an event-triggered control (ETC) protocol in order to only transmit data packets when some event-based conditions are satisfied, enabling to further reduce resource utilization such as bandwidth and energy consumption [36, 37, 38, 39, 40, 41]. Additionally, we provide a control design method based on the Cone Complementarity Linearization (CCL) algorithm [42] and Linear Matrix Inequalities (LMI) to design the predictor-feedback weighting factors and event-triggered parameters in order to enhance the closed-loop dynamic performance to the greatest extent.

The remainder of the paper is organized as follows: the problem statement is given in Section 2. The proposed weighted predictor-feedback control is presented in Section 3. The stability analysis and control synthesis are addressed in Section 4 and Section 5 respectively. Simulation results are provided in Section 6. Finally, some concluding remarks are gathered in Section 7.

2. Problem statement

Consider the following discrete-time interconnected system:

$$\begin{aligned} x_{i,k+1} &= \tilde{A}_{i,k}x_{i,k} + \tilde{B}_{i,k}u_{i,k-h_i} + \sum_{j=1,j\neq i}^{N} \tilde{F}_{ij,k}x_{j,k}, \\ x_{i,0} &= \theta_i,\ u_{i,\kappa} = \phi_i(\kappa), \quad \kappa = -h_i, -h_i+1, \cdots, 0 \end{aligned} \tag{1}$$

where $i \in \{1, ..., N\}$ is the subsystem index, $h_i \geq 0$ are the input delays, $x_{i,k} \in \mathcal{R}^{n_i}$ and $u_{i,k} \in \mathcal{R}^{m_i}$ are respectively the state and the local control input of the i^{th} subsystem with n_i and m_i the number of states and inputs respectively, $\tilde{A}_{i,k} \in \mathcal{R}^{n_i \times n_i}$ is the state transition matrix, $\tilde{B}_{i,k} \in \mathcal{R}^{n_i \times m_i}$ is the input matrix, and $\tilde{F}_{ij,k} \in \mathcal{R}^{n_i \times n_j}$ are coupling matrices. Terms θ_i, and $\phi_{i,\kappa}$ represent the initial conditions for the system state $x_{i,k}$ and the control input $u_{i,k}$. All system matrices $\tilde{A}_{i,k}$, $\tilde{B}_{i,k}$ and $\tilde{F}_{ij,k}$ in (1) are subjected to additive time-varying uncertainties described by the classical norm-bounded form [43]:

$$\begin{aligned} &\left(\tilde{A}_{i,k}, \tilde{B}_{i,k}\right) = (A_i, B_i) + J_i\Delta_{i,k}\left(H_i^A, H_i^B\right), \\ &\tilde{F}_{ij,k} = F_{ij} + J_i\Delta_{ij,k}H_j^F, \\ &i \neq j, \quad j \in \{1, ..., N\} \end{aligned} \tag{2}$$

where $A_i, B_i, F_{ij} \in \mathcal{R}^{n_i \times n_i}$, $J_i \in \mathcal{R}^{n_i \times l_{1,i}}$, $H_i^A, H_i^F \in \mathcal{R}^{l_{2,i} \times n_i}$, $H_i^B \in \mathcal{R}^{l_{2,i} \times m_i}$, $1 \leq i \leq N$ are known time-constant matrices, and $\Delta_{i,k}$, $\Delta_{ij,k}$ are unknown real and possibly time-varying matrices of appropriate dimensions such that $\Delta_{i,k}^T\Delta_{i,k} \leq I, \forall i \in \{1, ..., N\}$, and $\Delta_{ij,k}^T\Delta_{ij,k} \leq I$, $(i, j) \in \{1, ..., N\} \times \{1, ..., N\}, j \neq i$, $\forall k \geq 0$.

Definition 1. *The interconnected system* (1) *is said to be robustly exponentially stable with decay rate* β *if the overall system state* $x_k = \begin{bmatrix} x_{1,k}^T & \cdots & x_{N,k}^T \end{bmatrix}^T$ *satisfies* $||x_k|| \leq \mathcal{B}||x_0||\beta^k$, $\forall k \geq 0$ *for some* $\mathcal{B} > 1$ *and any initial state condition* $x_0 = \begin{bmatrix} x_{1,0}^T & \cdots & x_{N,0}^T \end{bmatrix}^T$.

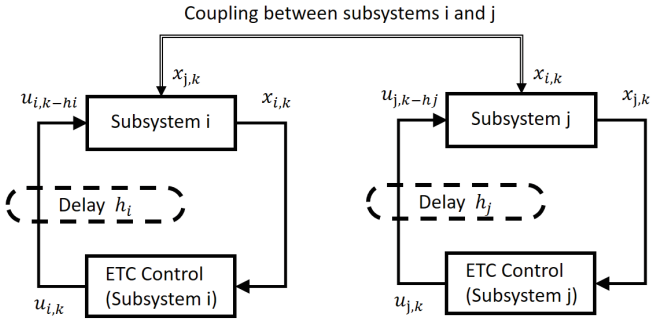

Figure 1: Block diagram of the closed-loop interconnected system with a distributed event-triggered control (ETC) scheme.

The objective is to design an ETC distributed predictor-feedback delay compensation scheme $u_{i,k},\ i = 1, ..., N$ (see Fig. 1) in order to stabilize the interconnected system (1) and improve the closed-loop performance to the greatest extent.

3. Event-triggered weighted predictor feedback control

Consider the distributed event-triggered control:

$$u_{i,k} = \begin{cases} \tilde{u}_{i,k} & \text{if (4) is true} \\ u_{i,k-1} & \text{otherwise,} \end{cases} \tag{3}$$

where $\tilde{u}_{i,k}$ is later defined in (5), and the event-triggering condition given below in (4) is used to decide whether the control action $u_{i,k}$ must be sent via network to the actuator:

$$\left(\tilde{u}_{i,k} - u_{i,k-1}\right)^T \Omega_i \left(\tilde{u}_{i,k} - u_{i,k-1}\right) \geq \sigma_i \tilde{u}_{i,k}^T \Omega_i \tilde{u}_{i,k}, \tag{4}$$

where $\Omega_i = \Omega_i^T \in \mathcal{R}^m > 0,\ i \in \{1, ..., N\}$ and the scalars $\sigma_i \geq 0$ are the event-triggered thresholds. Control actions will be transmitted if the relative difference between one control action and the last one is sufficiently high depending on Ω_i and σ_i, that is to say, if (4) is true. Note that $\sigma_i = 0$ corresponds to a time-triggered control scheme, which means that all control actions are transmitted at each sampling period. The average percentage of transmitted control actions with respect to the total number of sampling periods will be reduced as long as σ_i is higher, but at the expense of deteriorating the closed-loop performance. Hence, the existing compromise between

closed-loop dynamics performance and number of data transmissions can be adjusted by properly choosing σ_i, as discussed later in Example 2.

The proposed weighted predictor-feedback local controller $\tilde{u}_{i,k}$ with the above ETC scheme (3) is defined as:

$$\tilde{u}_{i,k} = K_i \left(A_i^{h_i} x_{i,k} + W_i \Phi_{i,k} \right), \qquad i \in \{1, ..., N\}, \tag{5}$$

where $K_i \in \mathcal{R}^{m_i \times n_i}$ and $W_i \in \mathcal{R}^{n_i \times n_i}$ are respectively the controller gains, and the weighting factors for each local prediction term $\Phi_{i,k}$, defined as:

$$\Phi_{i,k} = \sum_{j=1}^{h_i} A_i^{j-1} B_i \tilde{u}_{i,k-j}. \tag{6}$$

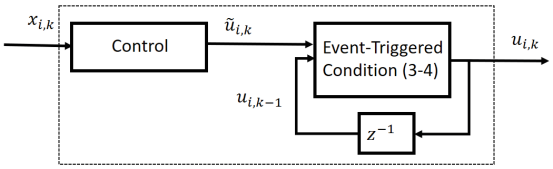

Figure 2: Event-triggered control (ETC) scheme defined in (3) and (4), where z^{-1} denotes a one-step delay.

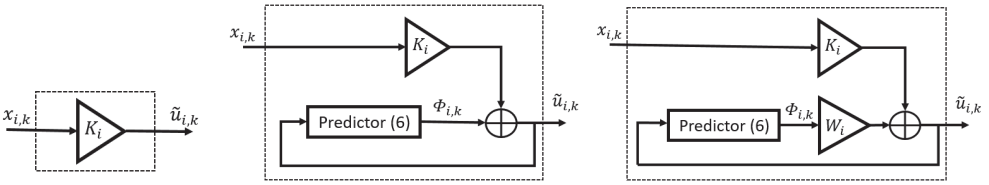

(a) NDC control (b) PF-DC control (c) WPF-DC control

Figure 3: Different control schemes: (a) No delay compensation (NDC), (b) Predictor-feedback delay compensation (PF-DC) and (c) Weighted predictor-feedback delay compensation (WPF-DC), where the prediction scheme $\Phi_{i,k}$ is shown below in Fig. 4

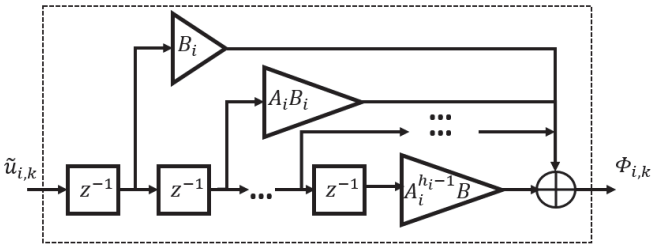

Figure 4: Prediction scheme defined in (6)

A block diagram of the above described control is represented in Fig. 2, Fig. 3c and Fig 4. The ETC scheme and the weighted predictor feedack control are depicted in Fig. 2 and Fig. 3c respectively (Fig. 3a and Fig. 3b correspond to a state-feedback control without delay compensation and a non-weighted predictor-feedback control respectively). Fig. 4 represents the block diagram of the prediction scheme used in Fig. 3b and Fig. 3c, which is defined in (6).

Remark 1. *Differently from other predictor-feedback controllers, we have introduced the parameters W_i to weight the relative importance of prediction components $\Phi_{i,k}$ in the control law* (5)*. Note that the state-feedback control scheme with no delay compensation (NDC) and the non-weighted predictor-feedback delay compensation (PF-DC) controller (see Fig. 3a and Fig. 3b) are both particular cases of the proposed weighted predictor-feedback control (WPF-DC) given in Fig. 3c by setting $W_i = 0$ and $W_i = I$ respectively. Hence, the weighting factors W_i bring extra degree of freedom for control synthesis (discussed later in Section 5), which may be helpful to improve the closed-loop performance.*

4. Exponential stability analysis with decay rate performance

Before addressing the stability analysis (Theorem 1 given below), an equivalent state-space model for the interconnected system (1) with the proposed control (3) is next obtained by means of the Artstein's reduction method [16]. Define:

$$z_{i,k} = A_i^{h_i} x_{i,k} + W_i \Phi_{i,k}, \tag{7}$$

where $x_{i,k}$ is the local state of each system, and W_i, $\Phi_{i,k}$ are respectively the weighting factor to be designed later and the prediction term defined in (6).

The one-step ahead of $z_{i,k}$ yields $z_{i,k+1} = A_i^{h_i} x_{i,k+1} + W_i \Phi_{i,k+1}$. Replacing $x_{i,k+1}$ from (1), we obtain:

$$\begin{aligned} z_{i,k+1} &= A_i^{h_i} \left(\tilde{A}_{i,k} x_{i,k} + \tilde{B}_{i,k} u_{i,k-h_i} \right) \\ &+ A_i^{h_i} \sum_{j=1, j\neq i}^{N} \tilde{F}_{ij,k} x_{j,k} + W_i \Phi_{i,k+1} \end{aligned} \tag{8}$$

Note that the above expression can equivalently be written as:

$$\begin{aligned} z_{i,k+1} &= A_i^{h_i} \left(\tilde{A}_{i,k} x_{i,k} + \tilde{B}_{i,k} \tilde{u}_{i,k-h_i} \right) + \sqrt{\sigma_i} A_i^{h_i} \tilde{B}_{i,k} \rho_{i,k} \\ &+ A_i^{h_i} \sum_{j=1, j\neq i}^{N} \tilde{F}_{ij,k} x_{j,k} + W_i \Phi_{i,k+1} \end{aligned} \tag{9}$$

where

$$\rho_{i,k} = \frac{1}{\sqrt{\sigma_i}} \left(u_{i,k-h_i} - \tilde{u}_{i,k-h_i} \right) \tag{10}$$

Replacing into (8) the terms $\tilde{A}_{i,k}$, $\tilde{B}_{i,k}$ and $\tilde{F}_{ij,k}$ defined in (2), and taking into account from (7) that $A_i^{h_i} x_{i,k} = z_{i,k} - W_i \Phi_{i,k}$, the above expression (9) renders:

$$\begin{aligned} z_{i,k+1} &= A_i z_{i,k} - A_i W_i \Phi_{i,k} + A_i^{h_i} B_i \tilde{u}_{i,k-h_i} \\ &+ \sqrt{\sigma_i} A_i^{h_i} B_i \rho_{i,k} + A_i^{h_i} \sum_{j=1, j\neq i}^{N} F_{ij} A_j^{-h_j} \left(z_{j,k} - W_j \Phi_{j,k} \right) \\ &+ A_i^{h_i} J_i \Delta_{i,k} H_i^A A_i^{-h_i} \left(z_{i,k} - W_i \Phi_{i,k} \right) \\ &+ A_i^{h_i} J_i \Delta_{i,k} H_i^B \tilde{u}_{i,k-h_i} + \sqrt{\sigma_i} A_i^{h_i} J_i \Delta_{i,k} H_i^B \rho_{i,k} \\ &+ A_i^{h_i} J_i \sum_{j=1, j\neq i}^{N} \Delta_{ij,k} H_j^F A_j^{-h_j} \left(z_{j,k} - W_j \Phi_{j,k} \right) \\ &+ W_i \Phi_{i,k+1} \end{aligned} \tag{11}$$

From the definition of $\Phi_{i,k}$ given in (6), it can be deduced that

$$\Phi_{i,k+1} = A_i \Phi_{i,k} + B_i \tilde{u}_{i,k} - A_i^{h_i} B_i \tilde{u}_{i,k-h_i} \tag{12}$$

It is easy to deduce from the definition (7) that $\tilde{u}_{i,k}$ in (5) can be expressed as $\tilde{u}_{i,k} = K_i z_{i,k}$, leading to

$$\Phi_{i,k+1} = A_i \Phi_{i,k} + B_i K_i z_{i,k} - A_i^{h_i} B_i K_i z_{i,k-h_i} \tag{13}$$

Hence, applying the equivalence (13), the closed-loop system formed by (1) and (5) can be obtained from (11) as:

$$\begin{aligned} z_{i,k+1} &= \left(A_i + W_i B_i K_i + A_i^{h_i} J_i \Delta_{i,k} H_i^A A_i^{-h_i}\right) z_{i,k} \\ &+ \left((I_{n_i} - W_i) A_i^{h_i} B_i + A_i^{h_i} J_i \Delta_{i,k} H_i^B\right) K_i z_{i,k-h_i} \\ &+ \left(W_i A_i - A_i W_i - A_i^{h_i} J_i \Delta_{i,k} H_i^A A_i^{-h_i} W_i\right) \Phi_{i,k} \\ &+ A_i^{h_i} \sum_{j=1, j\neq i}^{N} \left(F_{ij} + J_i \Delta_{ij,k} H_j^F\right) A_j^{-h_j} \left(z_{j,k} - W_j \Phi_{j,k}\right) \\ &- W_j \Phi_{j,k-h_i}) + \sqrt{\sigma_i} A_i^{h_i} \left(B_i + J_i \Delta_{i,k} H_i^B\right) \rho_{i,k} \end{aligned} \tag{14}$$

Finally, the closed-loop system (14), together with (13), can be written in compact form as:

$$\bar{\xi}_{k+1} = \tilde{\mathcal{A}}_k \bar{\xi}_k + \sum_{i=1}^{N} \tilde{\mathcal{M}}_{i,k} \bar{\xi}_{k-h_i} + \tilde{\mathcal{B}}_{\rho,k} \bar{\rho}_k \tag{15}$$

where

$$\begin{aligned} \bar{\xi}_k^T &= \left[z_{1,k}^T, \ \cdots, \ z_{N,k}^T, \ \Phi_{1,k}^T, \cdots, \ \Phi_{N,k}^T\right], \\ \bar{\rho}_k^T &= \left[\rho_{1,k}^T \ \cdots \ \rho_{N,k}^T\right], \\ \tilde{\mathcal{A}}_k &= \mathcal{A} + \mathcal{J} \bar{\Delta}_k \mathcal{H}, \\ \tilde{\mathcal{M}}_{i,k} &= \mathcal{M}_i + \mathcal{J}_i \bar{\Delta}_k \mathcal{H}_M, \\ \tilde{\mathcal{B}}_{\rho,k} &= \mathcal{B}_\rho + \mathcal{J} \bar{\Delta}_k \mathcal{H}_\rho, \end{aligned} \tag{16}$$

and

$$\mathcal{A} = \begin{bmatrix} \bar{A} + \bar{W}\bar{B}\bar{K} + \bar{A}_h\bar{F}\bar{A}_{-h} & \bar{W}\bar{A} - \bar{A}\bar{W} - \bar{A}_h\bar{F}\bar{A}_{-h}\bar{W} \\ \bar{B}\bar{K} & \bar{A} \end{bmatrix},$$

$$\mathcal{M}_i = \begin{bmatrix} \Gamma_i\left(I_{\bar{n}} - \bar{W}\right)\bar{A}_h\bar{B}\bar{K} & 0 \\ -\Gamma_i\bar{A}_h\bar{B}\bar{K} & 0 \end{bmatrix},$$

$$\mathcal{J} = \begin{bmatrix} 1 \\ 0 \end{bmatrix} \otimes \bar{A}_h\bar{J}, \quad \mathcal{J}_i = \begin{bmatrix} 1 \\ 0 \end{bmatrix} \otimes \Gamma_i\bar{A}_h\bar{J}, \quad \mathcal{B}_\rho = \begin{bmatrix} 1 \\ 0 \end{bmatrix} \otimes \bar{\sigma}\bar{B},$$

$$\mathcal{H} = \begin{bmatrix} \bar{H}\bar{A}_{-h} & -\bar{H}\bar{A}_{-h}\bar{W} \end{bmatrix}, \qquad \bar{\sigma} = diag_{i=1}^{N}\left(\sqrt{\sigma_i}\,\right),$$

$$\mathcal{H}_M = \begin{bmatrix} \bar{H}_B\bar{K} & 0 \end{bmatrix},$$

$$\mathcal{H}_\rho = diag_{i=1}^{N}\left(\sqrt{\sigma}_i H_i^B\right),$$

$$\Gamma_i = diag_{j=1}^{N}\left(\lambda_{ij} I_{n_i}\right), \qquad \lambda_{ij} = \begin{cases} 1 & \text{if } i == j \\ 0 & \text{otherwise,} \end{cases}$$

$$\bar{\Delta}_k = \begin{bmatrix} \Delta_{1,k} & \Delta_{12,k} & \cdots & \Delta_{1N,k} \\ \Delta_{21,k} & \Delta_{2,k} & \cdots & \Delta_{2N,k} \\ \cdots & \cdots & \cdots & \cdots \\ \Delta_{N1,k} & \Delta_{N2,k} & \cdots & \Delta_{N,k} \end{bmatrix} \tag{17}$$

where the symbol $\otimes$ stands for the Kronecker product, and

$$\bar{A} = diag_{i=1}^{N}\left(A_i\right), \qquad \bar{W} = diag_{i=1}^{N}\left(W_i\right), \tag{18}$$

$$\bar{B} = diag_{i=1}^{N}\left(B_i\right), \qquad \bar{K} = diag_{i=1}^{N}\left(K_i\right),$$

$$\bar{A}_h = diag_{i=1}^{N}\left(A_i^{h_i}\right), \qquad \bar{A}_{-h} = diag_{i=1}^{N}\left(A_i^{-h_i}\right),$$

$$\bar{J} = diag_{i=1}^{N}\left(J_i\right),$$

$$\bar{F} = \begin{bmatrix} 0 & F_{12} & \cdots & F_{1N} \\ F_{21} & 0 & \cdots & F_{2N} \\ \cdots & \cdots & \cdots & \cdots \\ F_{N1} & F_{N2} & \cdots & 0 \end{bmatrix}, \qquad \bar{H} = \begin{bmatrix} H_1^A & H_{12}^F & \cdots & H_{1N}^F \\ H_{21}^F & H_2^A & \cdots & H_{2N}^F \\ \cdots & \cdots & \cdots & \cdots \\ H_{N1}^F & H_{N2}^F & \cdots & H_N^A \end{bmatrix}$$

Theorem 1. *Given K_i, W_i and $\sigma_i > 0$, $i \in \{1, ..., N\}$ where N is the number of systems, the closed-loop system formed by* (1) *and the distributed weighted predictor-feedback ETC control* (3)-(5) *is β-stable if there exist symmetric matrices $P, Q_i, Z_i \in \mathcal{R}^{2\bar{n}} > 0$ with $\bar{n} = \sum_{i=1}^{N} n_i$, matrices $\Omega_i \in \mathcal{R}^{m_i} > 0$ and*

scalars $\varepsilon_i > 0$ such that the following LMI is satisfied [1]*:*

$$\begin{bmatrix} \Pi_1 & \Pi_2^T X & 0 & N\Pi_4^T \bar{E}_2 \\ (*) & -X & X\Pi_3 & 0 \\ (*) & (*) & -\bar{E}_1 & 0 \\ (*) & (*) & (*) & -\bar{E}_2 \end{bmatrix} < 0 \tag{19}$$

where [2]

$$\Pi_1 = \begin{bmatrix} \Pi_{11} & \Pi_{12} & 0 \\ (*) & -\bar{Q} - \bar{Z} & 0 \\ (*) & (*) & -\bar{\Omega} \end{bmatrix}, \; X = \begin{bmatrix} P & 0 & 0 \\ 0 & \mathcal{Z} & 0 \\ 0 & 0 & \bar{\Omega} \end{bmatrix}, \tag{20}$$

$$\Pi_2^T = \begin{bmatrix} \mathcal{A}^T & \mathcal{A}^T - I_{2\bar{n}} & 0 \\ \mathcal{M}^T & \mathcal{M}^T & \mathcal{K}^T \\ \mathcal{B}_\rho^T & \mathcal{B}_\rho^T & 0 \end{bmatrix}, \; \Pi_3 = \begin{bmatrix} \mathcal{J} & \bar{\mathcal{J}} \\ \mathcal{J} & \bar{\mathcal{J}} \\ 0 & 0 \end{bmatrix},$$

$$\Pi_4 = 1_{(N+1)\times 1} \otimes \begin{bmatrix} \mathcal{H} & 1_{1,N} \otimes \mathcal{H}_M & \mathcal{H}_\rho \end{bmatrix},$$

$$\Pi_{11} = -\beta^2 P + \sum_{i=1}^{N} \left(Q_i - \beta^{2h_i} Z_i \right) + \mathcal{L}_1^T \bar{S}_1 \mathcal{L}_1 - \mathcal{L}_2^T \bar{S}_2 \mathcal{L}_2,$$

$$\Pi_{12} = \begin{bmatrix} \beta^{2h_1} Z_1 & \cdots & \beta^{2h_N} Z_N \end{bmatrix},$$

$$\bar{E}_1 = diag_{i=1}^{N} \left(\varepsilon_i I_{N\bar{l}_1} \right), \qquad \bar{E}_2 = diag_{i=1}^{N} \left(\varepsilon_i I_{N\bar{l}_2} \right),$$

$$\bar{l}_1 = \sum_{i=1}^{N} l_{1,i}, \qquad \bar{l}_2 = \sum_{i=1}^{N} l_{2,i}$$

[1] The symbol $(*)$ stands for the corresponding terms induced by symmetry.

[2] The symbol $1_{m\times n}$ stands for a $m \times n$ matrix with all coefficients equal to 1.

and

$$
\begin{aligned}
&\mathcal{L}_1 = [1 \quad 0] \otimes I_{\bar{n}}, \qquad \mathcal{L}_2 = [0 \quad 1] \otimes I_{\bar{n}}, \\
&\bar{Q} = diag_{i=1}^{N}\left(\beta^{2h_i} Q_i\right), \qquad \bar{Z} = diag_{i=1}^{N}\left(\beta^{2h_i} Z_i\right), \\
&\bar{S}_1 = diag_{i=1}^{N}\left(\sum_{j=1}^{h_i} h_i \beta^{-2j} \left(A_i^{j-1} B_i K_i\right)^T S_i \left(A_i^{j-1} B_i K_i\right)\right), \\
&\bar{S}_2 = diag_{i=1}^{N}\left(S_i\right), \qquad \bar{\Omega} = diag_{i=1}^{N}\left(\Omega_i\right), \\
&\mathcal{Z} = \sum_{i=1}^{N} \gamma_i h_i Z_i, \qquad \gamma_i = \sum_{j=1}^{h_i} \beta^{2(j-1)}, \qquad i \in \{1, ..., N\}, \\
&\mathcal{M} = \begin{bmatrix} \mathcal{M}_1 & \cdots & \mathcal{M}_N \end{bmatrix}, \\
&\mathcal{K} = \bar{K} \cdot diag_{i=1}^{N}\left(u_i \otimes ([1 \quad 0] \otimes I_{n_i})\right), \\
&u_1 = [1,\ 0, \cdots, 0], u_2 = [0,\ 1, \cdots, 0], \cdots, u_N = [0,\ 0, \cdots,\ 1], \\
&\bar{\mathcal{J}} = \begin{bmatrix} \mathcal{J}_1 & \cdots & \mathcal{J}_N \end{bmatrix}
\end{aligned} \tag{21}
$$

with $\mathcal{M}_i, \mathcal{J}_i,\ i \in \{1, ..., N\}$ *defined in* (17).

Proof: See Appendix (Section 8) □

5. Control synthesis

This section provides a CCL-based algorithm to find the values of the weighting matrices W_i and the event-triggered parameters Ω_i of the proposed control scheme (3) with the objective to achieve faster convergence by minimizing the exponential decay rate β.

Before proceeding with the algorithm description, let us denote $\tilde{P} = P^{-1}$, $\tilde{\mathcal{Z}} = \mathcal{Z}^{-1}$, and $\tilde{X} = diag\left(\tilde{P},\ \tilde{\mathcal{Z}},\ \bar{\Omega}\right)$, By pre-and post multiplying (19) by $diag\left(I, \tilde{T}, I, I\right)$ with $\tilde{T} = diag\left(\tilde{P},\ \tilde{\mathcal{Z}},\ I\right)$, we obtain:

$$
\begin{bmatrix}
\Pi_1 & \Pi_2^T \mathcal{X} & 0 & N\Pi_4^T \bar{E}_2 \\
(*) & -\tilde{X} & \mathcal{X}\Pi_3 & 0 \\
(*) & (*) & -\bar{E}_1 & 0 \\
(*) & (*) & (*) & -\bar{E}_2
\end{bmatrix} < 0, \tag{22}
$$

where $\mathcal{X} = diag\left(I,\ I,\ \bar{\Omega}\right)$. Also, let us introduce the LMI conditions to relax the equality constraints $P\tilde{P} = I$ and $\mathcal{Z}\tilde{\mathcal{Z}} = I$ for the CCL algorithm:

$$\begin{bmatrix} P & I \\ I & \tilde{P} \end{bmatrix} \geq 0, \quad \begin{bmatrix} \mathcal{Z} & I \\ I & \tilde{\mathcal{Z}} \end{bmatrix} \geq, \tag{23}$$

together with the objective function to minimize:

$$\min(\text{trace}(P\tilde{P} + \tilde{P}P + \mathcal{Z}\tilde{\mathcal{Z}} + \tilde{\mathcal{Z}}\mathcal{Z})). \tag{24}$$

5.1. CCL algorithm description

The detailed CCL-algorithm is described as follows:

- Step (i): Solve the LMI's given in Theorem 1 for $\beta = \beta^{(0)}$ and $W_i = W_i^{(0)}$ for some initial values $\beta^{(0)}$, $W_i^{(0)}$, $i \in \{1, ..., N\}$. If a feasible solution is obtained, set $q := 0$, $P^{(q)} := P^{(q-1)}$, $\tilde{P}^{(q)} := \left(P^{(q-1)}\right)^{-1}$, $\mathcal{Z}^{(q)} := \mathcal{Z}^{(q-1)}$, $\tilde{\mathcal{Z}}^{(q)} := \left(\mathcal{Z}^{(q-1)}\right)^{-1}$ and go to Step (ii). Otherwise, increment $\beta^{(0)}$ until a feasible solution is found in Step (i).

- Step (ii): Solve the LMI's (22) and (23) subjet to

$$\min(\text{trace}(P\tilde{P}^{(q)} + \tilde{P}P^{(q)} + Z\tilde{Z}^{(q)} + \tilde{Z}Z^{(q)})) \tag{25}$$

  where $\beta = \beta^{(q)} - \delta_\beta$, being δ_β an incremental value for each iteration. Matrices $P, Q, Z_i, S_i, \Omega_i > 0$, together with the weigthing factors W_i are defined in this step as LMI decision variables.

- Step (iii): If a feasible solution is found, go to step (iv). Otherwise, set $\delta_\beta = \delta_\beta/\tau_\beta$ for some $\tau_\beta > 1$ until a feasible solution is found in Step (ii).

- Step (iv): If (19) holds with the obtained values in Step (iii): $W_i = W_i^{(q)}$, $\Omega_i = \Omega_i^{(q)}$, go to Step (v). Otherwise, set $\delta_\beta = \delta_\beta/\tau_\beta$ for some $\tau_\beta > 1$, and execute Steps (iii),(iv) until a feasible solution is found in step (iv).

- Step (v): If the maximum number of iterations is still not reached and $|\delta_\beta| > \epsilon_\beta$, being $\epsilon_\beta > 0$ a prescribed tolerance for stopping condition, set $q := q + 1$, $P^{(q)} := P^{(q-1)}$, $\tilde{P}^{(q)} := \left(P^{(q-1)}\right)^{-1}$, $Z^{(q)} := Z^{(q-1)}$, $\tilde{Z}^{(q)} := \left(Z^{(q-1)}\right)^{-1}$, $\beta^{(q)} := \beta^{(q-1)}$ and go to Step (ii). Otherwise, stop and exit.

6. Simulation results

This section presents three examples in order to validate the effectiveness of the proposed method. The first example illustrates that the proposed WPF-DC method can stabilize the system for larger delays than NDC and PF-DC, even in the case that NDC and PF-DC fail. The second example shows the comparative benefits of using WPF-DC with respect to NDC and PF-DC with ETC in terms of reduction of the average number of transmitted data. The third example shows the effectiveness of the proposed control synthesis algorithm to stabilize two strong coupled inverted pendulums that cannot be stabilized using NDC or PF-DC.

6.1. Example 1

Consider the interconnected system (1) formed by N unstable plants with system matrices $\tilde{A}_{1,k} \equiv 1.1$, $\tilde{B}_{i,k} \equiv 1$, and $\tilde{F}_{ij,k} = \gamma$, $(i,j) \in \{1,...,N\} \times \in \{1,...,N\}, j \neq i$, where $\gamma \geq 0$ describes the coupling strength between all subsystems. Let us consider the following three control schemes:

- (i) No Delay Compensation (NDC) ($W_i = 0, \forall i \in \{1,...,N\}$ in (5)).
- (ii) Predictor-feedback Delay Compensation (PF-DC) ($W_i = 1, \forall i \in \{1,...,N\}$ in (5)).
- (iii) Weighted predictor-feedback Delay Compensation (WPF-DC).

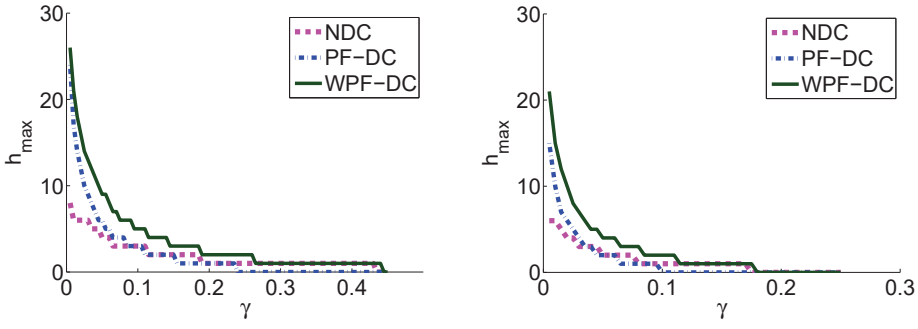

(a) h_{max} $(N = 3)$ (b) $h_{max}(N = 6)$

Figure 5: Comparison of the maximum allowable delay h_{max} for closed-loop stability as a function of the coupling factor γ that can be reached using NDC, PF-DC and WPF-DC for system given in Example 1 with (a) $N = 3$, (b) $N = 6$.

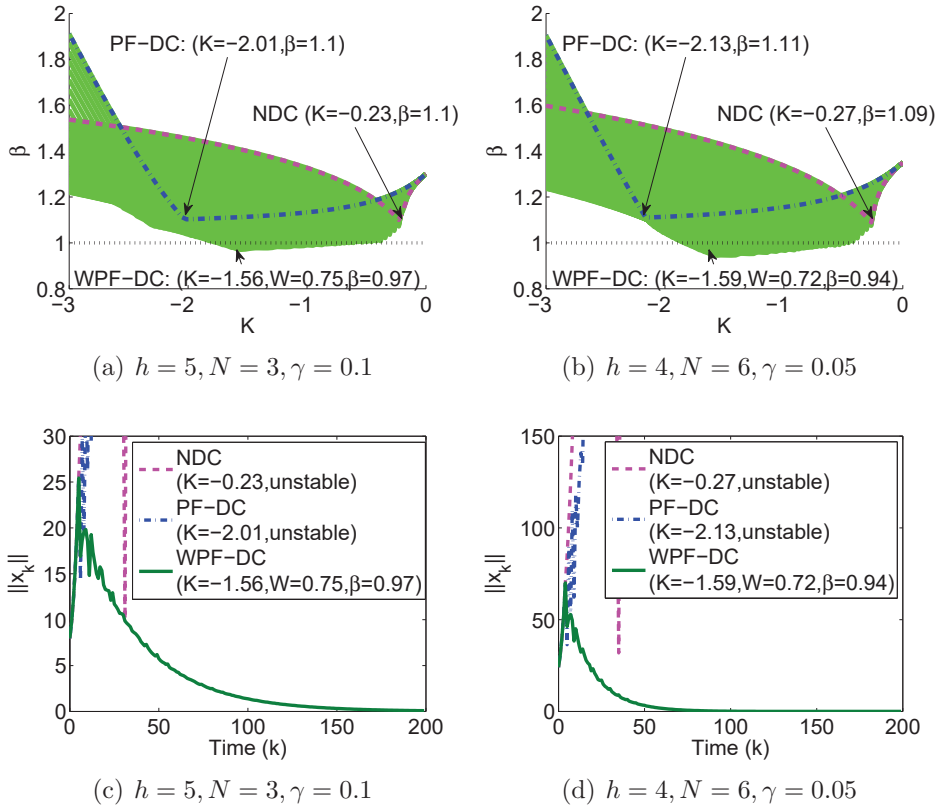

(a) $h = 5, N = 3, \gamma = 0.1$ (b) $h = 4, N = 6, \gamma = 0.05$

(c) $h = 5, N = 3, \gamma = 0.1$ (d) $h = 4, N = 6, \gamma = 0.05$

Figure 6: (a) and (b): Exponential decay rate β vs K obtained from the control schemes NDC, PF-DC and WPF-DC. (c) and (d): Time evolution of the closed-loop state $||x_k||$ for each control design.

In this example, we will consider the time-triggered version by choosing $\Omega_i = 1$ and $\sigma_i = 0$, $\forall i$, so we have that $u_{i,k} = \tilde{u}_{i,k}$. Since all subsystems have the same dynamics, we choose $K_i = K$, $W_i = W$ and $h_i \equiv h$ in order to simplify our analysis.

Let h_{max} be the maximum allowable delay such that the interconnected system is stable $\forall h \leq h_{max}$. The maximum allowable delay h_{max} that can be reached using the three above control schemes as a function of the coupling factor γ has been depicted in Fig. 5a and Fig. 5b for $N = 3$ and $N = 6$ respectively. It can be appreciated that WPF-DC can tolerate larger delays than NDC and PF-DC. The maximum allowable delay h_{max} has been analytically obtained by searching the maximum delay value h such that the

minimum spectral radius of the augmented closed-loop matrix (equivalent to the decay rate β) is less than one.

Fig. 6a and Fig. 6b compare the achieved decay rate β as a function of K using non-predictor (NDC: blue dashed line), predictor-feedback (PF-DC: red dash-dotted line), and the proposed weighted predictor-feedback (WPF-DC: solid green lines for different values of $0 \leq W \leq 1$). Two different cases have been studied in this example: ($h = 5, N = 3, \gamma = 0.1$ in Fig. 6a) and ($h = 4, N = 6, \gamma = 0.05$ in Fig. 6b). Note that in both cases, the system cannot be stabilized using NDC and PF-DC for any K (minimum decay rate β is always greater than 1). Nevertheless, the system can be stabilized by WPF-DC with $K = -1.56,\ W = 0.75$, obtaining $\beta = 0.97$ in the first case (Fig. 6a), and $K = -1.59,\ W = 0.72$ obtaining $\beta = 0.94$ in the second case (Fig. 6b). Hence, we have shown that the proposed control scheme can stabilize the system in two cases where both NDC and PF-DC fail.

To confirm this, simulation results of the state evolution have been depicted in Fig. 6c and Fig. 6d using the three control designs pointed out by text arrows in Fig. 6a and Fig. 6b. It can be observed that, contrary to NDC (dashed red line) and PF-DC (dotted blue line), the proposed WPF-DC scheme (solid green line) stabilizes the closed-loop system with an approximate 5%-error settling time of $\log(0.05)/\log(\beta) \approx 100$ sampling periods in Fig. 6a ($\beta = 0.97$) and $\log(0.05)/\log(\beta) \approx 50$ sampling periods in Fig. 6b ($\beta = 0.94$).

6.2. Example 2

Consider an interconnected system with three input delayed plants with time-varying model uncertainties: $\tilde{A}_{i,k} = 1.1 + \mu\Delta_{i,k},\ \tilde{B}_{i,k} = 1 + \mu\Delta_{i,k},\ i = 1, 2, 3,\ \tilde{F}_{ij,k} = 0.1(1 + \mu\Delta_{ij,k}),\ (i, j) \in [1, 2, 3] \times [1, 2, 3], j \neq i$ and input delays $h_i = 3$, where $\mu \geq 0$ determines the size of uncertanties, and $\Delta_{i,k},\ \Delta_{ij,k}$ are unknown time-varying parameters satisfying $|\Delta_{i,k}| \leq 1$ and $|\Delta_{ij,k}| \leq 1,\ \forall k \geq 0,\ \forall i, j \in \{1, ..., N\} \times \{1, ..., N\}$.

Control scheme	K	W	β_{min}
NDC	-0.23	0	0.98
PF-DC	-1.75	1	0.92
WPF-DC (proposed)	**-1.41**	**0.85**	**0.85**

Table 1: Different controller schemes designed to achieve the fastest convergence and the obtained minimum decay rate β_{min} (Example 2)

Following the same procedure as in the previous example, stabilizing controllers are designed using NDC, PF-DC and WPF-DC. As can be appreciated in Table 1, the faster convergence (minimum decay rate $\beta_{min} = 0.85$) is achieved by WPF-DC (bold-face row), where the controller parameters K and W designed for each case are depicted in columns 2 and 3.

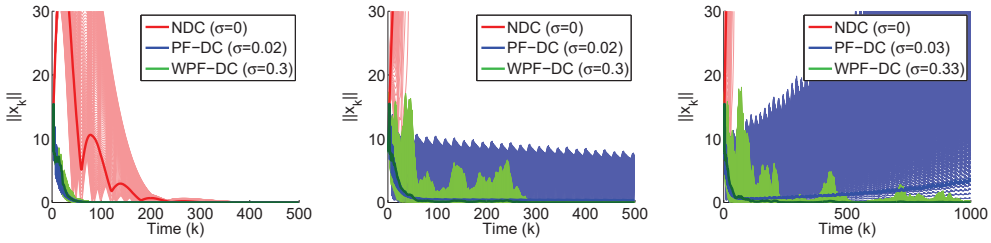

(a) $\mu = 0.005$ (b) $\mu = 0.04$ (c) $\mu = 0.04$

Figure 7: Comparison of the state evolution between the controllers given in Table 1 after 100 simulations for various μ and σ (Example 2) . The solid lines represent the average value for each case and the shadow regions represent the different state trajectories.

Control	$\mu = 0.005$	$\mu = 0.04$	$\mu = 0.04$
NDC	100% ($\sigma = 0$)	100%($\sigma = 0$) Unstable	100%($\sigma = 0$) Unstable
PF-DC	[99.87% − 99.94%] ($\sigma = 0.02$)	[97.72% − 98.84%] ($\sigma = 0.02$)	[97.18% − 98.24%] ($\sigma = 0.03$) Unstable
WPF-DC	[**65.97**% − **67.05**%] ($\sigma = 0.3$)	[**66.66**% − **68.38**%] ($\sigma = 0.3$)	[**64.98 % - 66.52**%] ($\sigma = 0.33$)

Table 2: Percentage of transmitted data (expressed as the 95%-confidence interval, t-value=2.22) obtained with the control schemes given in Table 1 after running 100 simulations for different values of μ and σ (Example 2)

Fig. 7a compares the different state evolutions using the three above controllers after performing 100 simulations for each one by considering model uncertainties of size $\mu = 0.005$ and different uncorrelated random sequences to generate time-varying patterns for $\Delta_{i,k} \in (-1, 1)$ and $\Delta_{ij,k} \in (-1, 1)$ in each simulation. The solid lines (NDC, red color; PF-DC, blue color;

WPF-DC, green color) represent the average value of all system trajectories, and the shadow region is the overlapping of the different system trajectories achieved in all simulations. For simulation results given in Fig. 7a, the NDC has been implemented using time-triggered ($\sigma = 0$), but PF-DC and WPF-DC have been implemented with ETC scheme by choosing $\sigma = 0.02$ and $\sigma = 0.3$ respectively. As a result, we obtain the percentage of transmitted data: $[99.87\% - 99.94\%]$ with PF-DC (thereafter expressed as the 95%-confidence interval, t-value=2.22), and $[65.97\% - 67.05\%]$ with WPF-DC, respectively (see Table 2, second column). Hence, WPF-DC achieve a significant reduction of the number of transmitted data packets (from an average of 99.9% to 66.5%) by keeping almost the same dynamic performance as PF-DC.

Now, let us increase the size of model uncertainties to $\mu = 0.04$. It can be appreciated in Fig. 7b that NDC (red color) becomes unstable and PF-DC (blue color) exhibits slow convergence, whereas WPF-DC (green color) keeps comparatively a reasonable convergence rate. Note that the percentage of transmitted data are quite similar as the previous case: $[97.72\% - 98.84\%]$ with PF-DC and $[66.66\% - 68.38\%]$ with WPF-DC, respectively (see Table 2, third column).

Fig. 7c performs the same comparison as Fig. 7b with $\mu = 0.04$ but slightly increasing the value of σ in PF-DC (from $\sigma = 0.02$ to $\sigma = 0.03$) and WPF-DC (from $\sigma = 0.3$ to $\sigma = 0.33$). In this case both NDC and PF-DC are unstable, but WPF-DC still keeps stable but close to the verge of instability. In both cases, the number of trasmissions is also quite similar as previous cases: $[97.18\% - 98.24\%]$ for PF-DC and $[64.98\% - 66.52\%]$ for WPF-DC respectively $[97.18\% - 98.24\%]$.(see Table 2, fourth column). Hence, it has been illustrated that WPF-DC can achieve larger reduction of data transmissions and better trade-off between robust performance and bandwidth consumption in comparison to NDC and PF-DC.

6.3. Example 3

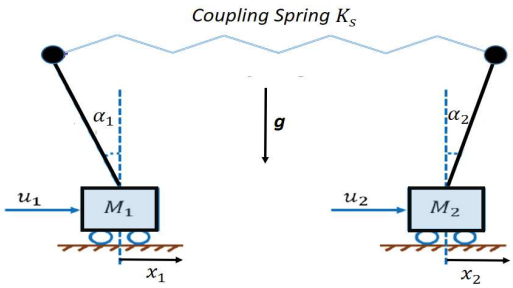

[t!]

Figure 8: Two coupled inverted pendulums on two carts (Example 3).

In this example, we study the example already proposed in [2, 35] which consists in two coupled inverted pendulums on two carts (see Fig 8). After discretization with sampling time $T_s = 50ms$, the interconnected time delay system model can be described by (1) with system matrices:

$$A_1 = A_2 = \begin{bmatrix} 1.00 & 0.05 & 0 & 0 \\ 0.15 & 1.00 & 0 & 0 \\ 0 & 0 & 1.00 & 0.05 \\ -0.08 & 0 & 0 & 1.00 \end{bmatrix}, \; B_1 = B_2 = 10^{-3} \cdot \begin{bmatrix} 0 \\ -0.21 \\ 0 \\ 0.83 \end{bmatrix}^T,$$

$$F_{12} = F_{21} = \gamma \begin{bmatrix} 0 & 0 & 0 & 0 \\ 0.02 & 0 & 0.01 & 0 \\ 0 & 0 & 0 & 0 \\ -0.01 & 0 & -0.01 & 0 \end{bmatrix}$$

where $\gamma > 0$ is a scalar that describes the coupling strength between both inverted pendulums. The stabilizing controller gains are chosen as [2, 35]:

$$\begin{aligned} K_1 &= 10^4 \cdot \begin{bmatrix} 1.1308 & 0.7144 & 0.0574 & 0.1198 \end{bmatrix}, \\ K_2 &= 10^4 \cdot \begin{bmatrix} 2.9023 & 1.8007 & 0.2873 & 0.3691 \end{bmatrix}. \end{aligned} \tag{26}$$

Let $h_i = 5, \; i = 1, 2$. Differently from [2, 35], the coupling strength between both inverted pendulums is increased to $\gamma = 303$ to force the system to closed-loop instability with NDC and WPF-DC controllers. The objective is to find a stabilizing controller using WPF-DC.

To this end, two different WPF-DC stabilizing controllers have been obtained by CCL-based Algorithm (see Section 5.1). The first one has been obtained after 14 iterations by setting $\sigma_i = 0,\ i = 1, 2$ (time-triggered scheme) and other CCL parameters as $W_1^{(0)} = W_2^{(0)} = I$, $\beta^{(0)} = 1.3$, $\delta_\beta = 0.1$, $\tau_\beta = 2$, $\epsilon_\beta = 10^{-4}$ and $\sigma_1 = \sigma_2 = 0$. As a result, a stabilizing controller is obtained with guaranteed exponential decay rate decay rate $\beta = 0.9999314$ and the following weighting factors:

$$W_1 = \begin{bmatrix} -0.4548 & 0.8679 & -0.1159 & 0.1693 \\ 2.8766 & -0.7292 & 0.1042 & -0.4364 \\ 0.9988 & -1.4330 & 1.0191 & -0.4116 \\ -4.1495 & 1.2132 & 1.5267 & 1.2194 \end{bmatrix}, \tag{27}$$

$$W_2 = \begin{bmatrix} 0.3057 & 0.6856 & -0.0826 & 0.1698 \\ 2.4498 & 0.2260 & 0.0805 & -0.1479 \\ 0.5968 & -0.6738 & 1.1598 & -0.2591 \\ -3.9114 & 0.2065 & 1.1310 & 0.8400 \end{bmatrix}$$

The second WPF-DC stabilizing controller has been obtained with the same algorithm and CCL parameters setting, but considering the largest σ ($\sigma = 0.17$) that allows a feasible solution. As a result, we have obtained after 15 iterations with guaranteed exponential decay rate $\beta = 0.999971$. The new designed weighting factors, together with the event-triggered parameters, are depicted below:

$$W_1 = \begin{bmatrix} -0.4304 & 0.0818 & -0.1469 & -0.0188 \\ 0.5655 & -0.4776 & -0.3671 & -0.2935 \\ 0.3397 & -0.6364 & 0.8356 & -0.2517 \\ -1.7230 & 0.8018 & 1.7514 & 0.7671 \end{bmatrix}, \tag{28}$$

$$W_2 = \begin{bmatrix} 0.3896 & 0.1166 & -0.0873 & 0.0266 \\ -0.6282 & 0.1826 & -0.8762 & -0.0616 \\ -1.2456 & -0.5106 & 0.7139 & -0.2233 \\ 3.4734 & 0.6210 & 3.8938 & 0.5060 \end{bmatrix},$$

$$\Omega_1 = 1517.7, \qquad \Omega_2 = 277.9, \qquad \sigma = 0.17$$

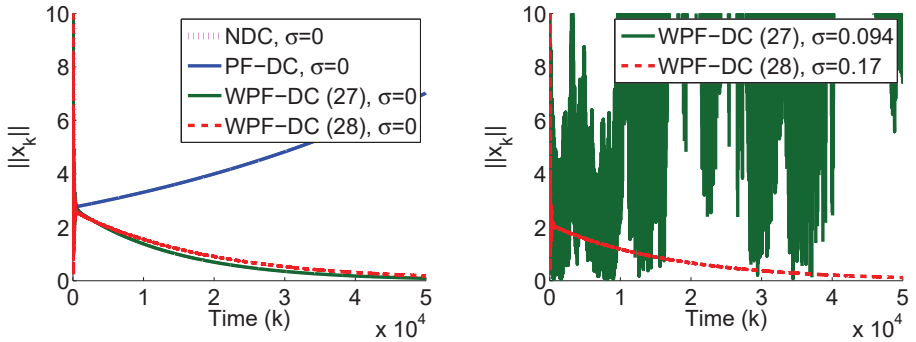

(a) Time-triggered ($\sigma = 0$) (b) Event-triggered ($\sigma > 0$)

Figure 9: (a) Comparison of the state evolution between NDC, PF-DC and WPF-DC with W_1, W_2 given in (27) and (28) with $\sigma = 0$ in all three cases. (b) Comparison of the state evolution between WPF-DC (27) ($\sigma = 0.09$) and WPF-DC (28) ($\sigma = 0.17$).

Comparative simulation results are depicted in Fig. 9a using time-triggered scheme ($\sigma = 0$), where it can be appreciated that NDC and PF-DC become unstable, meanwhile the proposed WPF-DC (5) with the designed weighting factors in (27) and (28) stabilizes the interconnected system.

Fig 9b compares the average closed-loop response obtained with the event-triggered scheme for WPF-DC (28) (solid red line, $\sigma = 0.17$) and WPF-DC (27) (green dash-dotted line, $\sigma = 0.094$) after running 10 time simulations and considering different initial conditions in each case. As expected from the second CCL Algorithm design (28), it can be appreciated that WPF-DC (28) is stable with a similar transient response as Fig. 9a, but achieving a significant reduction of transmitted data: $[30.34\% - 30.53\%]$. However, the closed-loop response with WPF-DC (27) becomes unstable although the number of data transmissions is bigger in comparison to WPF-DC (28) ($[38.84\% - 39.27\%]$ versus $[30.34\% - 30.53\%]$). This is due to the fact that WPF-DC (27) was designed for a time-triggered control ($\sigma = 0$). In this case, $\sigma = 0.094$ is just the maximum threshold that forces the system to instability. Therefore, the average number of transmission data cannot be further reduced with WPF-DC (27), whereas the designed event-triggered WPF-DC (28) with the proposed control design method can achieve larger reduction of transmission data keeping the stability.

7. Conclusions and perspectives

This paper has presented a novel distributed event-triggered predictor-feedback control for interconnected systems with input delays. New weighting factors for each local prediction term have been introduced, bringing extra degree of freedom for control synthesis. Moreover, we have provided a CCL-based algorithm to design the weighting factors, together with event-triggered parameters, to improve the convergence rate. Finally, simulation results have been provided to show that: (i) the control system can be stabilized by the proposed method even in the case that other control strategies fail (ii) not only faster convergence, but also larger delays, better robustness and less bandwidth consumption can be achieved in comparison to previous approaches. Future developments could address the research of output-feedback observer-predictor control strategies aimed at improving the compromise between complexity and performance.

8. Appendix: Proof of Theorem 1

Let us consider the Lyapunov-Krasovskii functional $V_k = V_{1,k} + V_{2,k} + V_{3,k} + V_{4,k}$, where:

$$V_{1,k} = \bar{\xi}_k^T P \bar{\xi}_k, \quad V_{2,k} = \sum_{i=1}^{N} \sum_{j=1}^{h_i} \beta^{2(j-1)} \bar{\xi}_{k-j}^T Q_i \bar{\xi}_{k-j}, \tag{29}$$

$$V_{3,k} = \sum_{i=1}^{N} h_i \left(\sum_{m=1}^{h_i} \sum_{j=1}^{m} \beta^{2(m-1)} \delta_{z,k-j}^T Z_i \delta_{z,k-j} \right),$$

$$V_{4,k} = \sum_{i=1}^{N} h_i \left(\sum_{m=1}^{h_i} \sum_{j=1}^{m} \beta^{2(j-1)} \eta_{i,k-j}^T(m) \; S_i \; \eta_{i,k-j}(m) \right)$$

where $\delta_{z,k} = \bar{\xi}_{k+1} - \bar{\xi}_k$ and

$$\eta_{i,k}(m) = \beta^{-m} A_i^{m-1} B_i K_i z_{i,k} \tag{30}$$

The system is β-stable if there exists $V_k > 0$ such that $V_{k+1} - \beta^2 V_k < 0$. Then, defining the forward difference $\Delta_\beta V_{l,k} = V_{l,k+1} - \beta^2 V_{l,k}$, $l = 1, 2, 3, 4$,

we have that:

$$
\begin{aligned}
\Delta_\beta V_{1,k} &= \bar{\xi}_k^T \tilde{\mathcal{A}}_k^T P \tilde{\mathcal{A}}_k \bar{\xi}_k \\
&+ 2\bar{\xi}_k^T \tilde{\mathcal{A}}_k^T P \left(\sum_{i=1}^{N} \tilde{\mathcal{M}}_{i,k} \bar{\xi}_{k-h_i} \right) + 2\bar{\xi}_k^T \tilde{\mathcal{A}}_k^T P \tilde{\mathcal{B}}_{\rho,k} \bar{\rho}_k \\
&+ \left(\sum_{i=1}^{N} \tilde{\mathcal{M}}_{i,k} \bar{\xi}_{k-h_i} \right)^T P \left(\sum_{i=1}^{N} \tilde{\mathcal{M}}_{i,k} \bar{\xi}_{k-h_i} \right) \\
&+ 2 \left(\sum_{i=1}^{N} \tilde{\mathcal{M}}_{i,k} \bar{\xi}_{k-h_i} \right)^T P \tilde{\mathcal{B}}_{\rho,k} \bar{\rho}_k + \bar{\rho}_k^T \tilde{\mathcal{B}}_{\rho,k}^T P \tilde{\mathcal{B}}_{\rho,k} \bar{\rho}_k - \beta^2 P, \qquad (31) \\
\Delta_\beta V_{2,k} &= \bar{\xi}_k^T \sum_{i=1}^{N} Q_i \bar{\xi}_k - \sum_{i=1}^{N} \beta^{2h_i} \bar{\xi}_{k-h_i}^T Q_i \bar{\xi}_{k-h_i}, \\
\Delta_\beta V_{3,k} &= \delta_{z,k}^T \mathcal{Z} \delta_{z,k} - \sum_{i=1}^{N} \beta^{2h_i} \left(h_i \sum_{j=1}^{h_i} \delta_{z,k-j}^T Z_i \delta_{z,k-j} \right), \\
\Delta_\beta V_{4,k} &= \sum_{i=1}^{N} h_i \left(\sum_{j=1}^{h_i} \eta_{i,k}^T(j) \; S_i \; \eta_{i,k}(j) \right) \\
&- \sum_{i=1}^{N} h_i \left(\sum_{j=1}^{h_i} \beta^{2j} \eta_{i,k-j}^T(j) S_i \eta_{i,k-j}(j) \right), \\
&= \bar{\xi}_k^T \left(\mathcal{L}_1^T \bar{S}_1 \mathcal{L}_1 \right) \bar{\xi}_k \\
&- \sum_{i=1}^{N} h_i \left(\sum_{j=1}^{h_i} \left(\beta^j \eta_{i,k-j}(j) \right)^T S_i \left(\beta^j \eta_{i,k-j}(j) \right) \right)
\end{aligned}
$$

Applying Jensen's inequality [44], from the rightmost part of $\Delta_\beta V_{3,k}$ and taking into account that $\sum_{j=1}^{h_i} \delta_{z,k-j} = \bar{\xi}_k - \bar{\xi}_{k-h_i}$, we obtain:

$$
\begin{aligned}
&- h_i \sum_{j=1}^{h_i} \delta_{z,k-j}^T Z_i \delta_{z,k-j} \\
&\leq - \left(\sum_{j=1}^{h_i} \delta_{z,k-j} \right)^T Z_i \left(\sum_{j=1}^{h_i} \delta_{z,k-j} \right) \\
&= - \left(\bar{\xi}_k - \bar{\xi}_{k-h_i} \right)^T Z_i \left(\bar{\xi}_k - \bar{\xi}_{k-h_i} \right) \qquad (32)
\end{aligned}
$$

Applying again Jensen's inequality, from the rightmost part of $\Delta_\beta V_{4,k}$ and taking into account that $\beta^j \eta_{i,k-j}(j) = A_i^{j-1} B_i K_i z_{i,k-j}$ and the definition of $\Phi_{i,k}$ in (6), we obtain that $\sum_{j=1}^{h_i} \beta^j \eta_{i,k-j}^T(j) = \Phi_{i,k}$, and therefore:

$$\begin{aligned} & -\sum_{i=1}^{N} h_i \left(\sum_{j=1}^{h_i} \left(\beta^j \eta_{i,k-j}(j)\right)^T S_i \left(\beta^j \eta_{i,k-j}(j)\right) \right) \\ & \leq -\sum_{i=1}^{N} \left(\sum_{j=1}^{h_i} \beta^j \eta_{i,k-j}^T(j) \right)^T S_i \left(\sum_{j=1}^{h_i} \beta^j \eta_{i,k-j}(j) \right) \\ & = -\sum_{i=1}^{N} \Phi_{i,k}^T S_i \Phi_{i,k} = -\bar{\xi}_k^T \left(\mathcal{L}_2^T \bar{S}_2 \mathcal{L}_2 \right) \bar{\xi}_k \end{aligned} \tag{33}$$

From (3) and (4), it can be deduced that the following condition always holds $\forall i \in \{1, ..., N\}$:

$$\begin{aligned} & \left(u_{i,k-h_i} - \tilde{u}_{i,k-h_i}\right)^T \Omega_i \left(u_{i,k-h_i} - \tilde{u}_{i,k-h_i}\right) \\ & \leq \sigma_i \tilde{u}_{i,k-h_i}^T \Omega_i \tilde{u}_{i,k-h_i} \end{aligned} \tag{34}$$

The above condition, together with the definition of $\rho_{i,k}$ given in (10), leads to:

$$\rho_{i,k}^T \Omega_i \rho_{i,k} \leq \tilde{u}_{i,k-h_i}^T \Omega_i \tilde{u}_{i,k-h_i} \tag{35}$$

which can equivalently be expressed as:

$$\rho_{i,k} = \Delta_{\rho,i,k} \tilde{u}_{i,k-h_i} \tag{36}$$

where $\Delta_{\rho,i,k} : \ \tilde{u}_{i,k} \rightarrow \rho_{i,k}, \ i \in \{1, ..., N\}$ are time-varying operators satisfying:

$$||\Omega_i^{1/2} \ \Delta_{\rho,i,k} \ \Omega_i^{-1/2}||_\infty \leq 1 \tag{37}$$

From the definition of $\bar{\rho}_k$ given in (16) and $\tilde{u}_{i,k} = K_i z_{i,k}$ (see (5) and (7)), we can write (36) in compact form as:

$$\bar{\rho}_k = \bar{\Delta}_{\rho,k} \bar{\omega}_k \tag{38}$$

where $\bar{\Delta}_{\rho,k} = diag_{i=1}^N \Delta_{\rho,i,k}$ and

$$\bar{\omega}_k = \bar{K} \left[z_{1,k-h_1}^T, \ \ \cdots, z_{N,k-h_N} \right]^T \tag{39}$$

with $\bar{K} = diag_{i=1}^{N} K_i$. Note from $\bar{\xi}_k$ and $\mathcal{L}_1$ defined in (16) and (21) that $\bar{z}_k = \mathcal{L}_1 \bar{\xi}_k$. Hence, $\bar{\omega}_k$ can also be reformulated as:

$$\bar{\omega}_k = \mathcal{K} \begin{bmatrix} \bar{\xi}_{k-h_1}^T & \cdots & \bar{\xi}_{k-h_i}^T \end{bmatrix} \tag{40}$$

where $\mathcal{K}$ is defined in (21). Then, given $\bar{\Omega} = diag_{i=1}^{N} \Omega_{i,k}$ and the above term $\bar{\Delta}_{\rho,k}$, it is easy to see that

$$||\bar{\Omega}^{1/2}\ \bar{\Delta}_{\rho,k}\ \bar{\Omega}^{-1/2}||_\infty \leq 1 \tag{41}$$

The negativeness of the forward difference $\Delta_\beta V_k = V_{k+1} - \beta^2 V_k = \sum_{l=1}^{4} \Delta_\beta V_{l,k}$ along trajectories of $\bar{\xi}_k$ with $\Delta_\beta V_{l,k},\ l = 1, 2, 3, 4$ given in (31), together with the fulfilment of the constraint (41), can be ensured by proving the inequality:

$$\Delta_\beta V_k + \bar{\omega}_k^T \bar{\Omega} \bar{\omega}_k - \bar{\rho}_k^T \bar{\Omega} \bar{\rho}_k < 0, \tag{42}$$

where $\bar{\Omega} = diag_{i=1}^{N} (\Omega_i)$ and $\bar{\rho}_k$, $\bar{\omega}_k$ are defined in (38) and (40) respectively. From (31) and the inequalities given in (32) and (33), we deduce that (42) can be expressed as $\bar{\chi}_k^T \Xi_k \bar{\chi}_k < 0$, where $\bar{\chi}_k$ is defined as

$$\bar{\chi}_k^T = \begin{bmatrix} \bar{\xi}_k^T & \bar{\xi}_{k-h_1}^T & \cdots & \bar{\xi}_{k-h_i}^T & \bar{\rho}_k \end{bmatrix} \tag{43}$$

and

$$\Xi_k = \Pi_1 + \tilde{\Pi}_{2,k}^T X \tilde{\Pi}_{2,k}, \tag{44}$$

where X is defined in (20), and

$$\tilde{\Pi}_{2,k}^T = \begin{bmatrix} \tilde{A}_k^T & \tilde{A}_k^T - I & 0 \\ \tilde{\mathcal{M}}_k^T & \tilde{\mathcal{M}}_k^T & \mathcal{K}^T \\ \tilde{B}_{\rho,k}^T & \tilde{B}_{\rho,k}^T & 0 \end{bmatrix} \tag{45}$$

with $\tilde{\mathcal{M}}_k = (\mathcal{M}_{1,k}, ..., \mathcal{M}_{N,k})$. Recalling the definitions of $\tilde{\mathcal{A}}_k$, $\tilde{\mathcal{M}}_{i,k}$ and $\tilde{\mathcal{B}}_{\rho,k}$ given in (16), we can write $\tilde{\Pi}_{2,k} = \Pi_2 + \Pi_3 \left(I_{N+1} \otimes \bar{\Delta}_k\right) \Pi_4$ with Π_2, Π_3, Π_4 defined in (20) and $\bar{\Delta}_k$ in (17). From (44) and applying Schur Complement, the above inequality $\bar{\chi}_k^T \Xi_k \bar{\chi}_k < 0$ is true $\forall \bar{\chi}_k \neq 0$ if and only if

$$\begin{bmatrix} \Pi_1 & \Pi_2^T X \\ X\Pi_2 & -X \end{bmatrix} + \left(\begin{bmatrix} 0 \\ X\Pi_3 \end{bmatrix} \left(I_{N+1} \otimes \bar{\Delta}_k\right) \begin{bmatrix} \Pi_4 & 0 \end{bmatrix} \right) + \left(\begin{bmatrix} 0 \\ X\Pi_3 \end{bmatrix} \left(I_{N+1} \otimes \bar{\Delta}_k\right) \begin{bmatrix} \Pi_4 & 0 \end{bmatrix} \right)^T < 0 \tag{46}$$

Note from the definition of $\Delta_{i,k}, \Delta_{ij,k}$ and $\bar{\Delta}_k$ in (2) and (17), we have that $||\bar{\Delta}_k||_\infty \leq N$. Applying the Petersen inequality [45] and defining $\tilde{\Delta}_k = \frac{1}{N}\left(I_{N+1} \otimes \bar{\Delta}_k\right)$, we have that there exists positive scalars $\varepsilon_i,\ i \in \{1, ..., N+1\}$ such that

$$\begin{aligned} &He\left(\begin{bmatrix} 0 \\ X\Pi_3 \end{bmatrix} \tilde{\Delta}_k \begin{bmatrix} N\Pi_4 & 0 \end{bmatrix}\right) \\ &+ \left(\begin{bmatrix} 0 \\ X\Pi_3 \end{bmatrix} \tilde{\Delta}_k \begin{bmatrix} N\Pi_4 & 0 \end{bmatrix}\right)^T \\ &\leq \begin{bmatrix} 0 \\ X\Pi_3 \end{bmatrix} \bar{E}_1^{-1} \begin{bmatrix} 0 & (X\Pi_3)^T \end{bmatrix} + \begin{bmatrix} N\Pi_4^T \\ 0 \end{bmatrix} \bar{E}_2 \begin{bmatrix} N\Pi_4 & 0 \end{bmatrix}, \end{aligned} \tag{47}$$

where $\bar{E}_1 > 0$ and $\bar{E}_2 > 0$ are defined in (20) and satisfy $\bar{E}_1\tilde{\Delta}_k = \tilde{\Delta}_k\bar{E}_2$. Hence, applying (47) and Schur Complement, we have that (47) is equivalent to

$$\begin{bmatrix} \Pi_1 & \Pi_2^T X & 0 & N\Pi_4^T \\ (*) & -X & X\Pi_3 & 0 \\ (*) & (*) & -\bar{E}_1 & 0 \\ (*) & (*) & (*) & -\bar{E}_2^{-1} \end{bmatrix} < 0 \tag{48}$$

Finally, pre- and post-muliplying the above inequality by $diag\left(I, I, I, \bar{E}_2\right)$ we obtain (19), concluding the proof.

Acknowledgement

This work was supported by projects PGC2018-098719-B-I00 (MCIU/ AEI/ FEDER, UE), Group DGA T45-17R and Fundacion Universitaria Antonio Gargallo (Project 2018/B004)

References

[1] S. Hu, D. Yue, J. Liu, H_∞ filtering for networked systems with partly known distribution transmission delays, Information Sciences 194 (2012) 270–282.

[2] D. P. Borgers, M. W. Heemels, Stability analysis of large-scale networked control systems with local networks: A hybrid small-gain approach, in: Proceedings of the 17th International Conference on Hybrid systems: Computation and Control, ACM, 2014, pp. 103–112.

[3] K.-Z. Liu, R. Wang, G.-P. Liu, Tradeoffs between transmission intervals and delays for decentralized networked control systems based on a gain assignment approach, IEEE Transactions on Circuits and Systems II: Express Briefs 63 (5) (2015) 498–502.

[4] K. Liu, A. Selivanov, E. Fridman, Survey on time-delay approach to networked control, Annual Reviews in Control.

[5] R. Yang, Y. Yu, J. Sun, H. R. Karimi, Event-based networked predictive control for networked control systems subject to two-channel delays, Information Sciences 524 (2020) 136–147.

[6] R. Olfati-Saber, R. M. Murray, Consensus problems in networks of agents with switching topology and time-delays, IEEE Transactions on Automatic Control 49 (9) (2004) 1520–1533.

[7] P.-A. Bliman, G. Ferrari-Trecate, Average consensus problems in networks of agents with delayed communications, Automatica 44 (8) (2008) 1985–1995.

[8] N. Huang, Z. Sun, B. D. Anderson, Z. Duan, Distributed and adaptive triggering control for networked agents with linear dynamics, Information Sciences 517 (2020) 297–314.

[9] Y. Yang, X.-M. Zhang, W. He, Q.-L. Han, C. Peng, Sampled-position states based consensus of networked multi-agent systems with second-order dynamics subject to communication delays, Information Sciences 509 (2020) 36–46.

[10] E. Fridman, Introduction to time-delay systems: Analysis and control, Springer, 2014.

[11] J. E. Normey-Rico, Control of dead-time processes, Springer Science & Business Media, 2007.

[12] I. Karafyllis, M. Krstic, Predictor feedback for delay systems: Implementations and approximations, Springer, 2017.

[13] H. Lhachemi, C. Prieur, R. Shorten, An LMI condition for the robustness of constant-delay linear predictor feedback with respect to uncertain time-varying input delays, Automatica 109 (2019) 108551.

[14] O. Smith, Closer control of loops with dead time, Chemical Engineering Progress 53 (5) (1959) 217–219.

[15] A. Manitius, A. Olbrot, Finite spectrum assignment problem for systems with delays, IEEE Transactions on Automatic Control 24 (4) (1979) 541–552.

[16] Z. Artstein, Linear systems with delayed controls: A reduction, IEEE Transactions on Automatic control 27 (4) (1982) 869–879.

[17] P. Garcia, A. Gonzalez, P. Castillo, R. Lozano, P. Albertos, Robustness of a discrete-time predictor-based controller for time-varying measurement delay, IFAC Proceedings Volumes 43 (2) (2010) 367–372.

[18] A. González, A. Sala, R. Sanchis, LK stability analysis of predictor-based controllers for discrete-time systems with time-varying actuator delay, Systems & Control Letters 62 (9) (2013) 764–769.

[19] S. Hao, T. Liu, B. Zhou, Output feedback anti-disturbance control of input-delayed systems with time-varying uncertainties, Automatica 104 (2019) 8–16.

[20] A. Selivanov, E. Fridman, Predictor-based networked control under uncertain transmission delays, Automatica 70 (2016) 101–108.

[21] B. Zhou, Z. Lin, G.-R. Duan, Truncated predictor feedback for linear systems with long time-varying input delays, Automatica 48 (10) (2012) 2387–2399.

[22] N. Bekiaris-Liberis, M. Krstic, Robustness of nonlinear predictor feedback laws to time-and state-dependent delay perturbations, Automatica 49 (6) (2013) 1576–1590.

[23] F. Mazenc, M. Malisoff, Stabilization of nonlinear time-varying systems through a new prediction based approach, IEEE Transactions on Automatic Control 62 (6) (2016) 2908–2915.

[24] I. Karafyllis, M. Krstic, Robust predictor feedback for discrete-time systems with input delays, International Journal of Control 86 (9) (2013) 1652–1663.

[25] M. S. Mahmoud, Y. Xia, A generalized approach to stabilization of linear interconnected time-delay systems, Asian Journal of Control 14 (6) (2012) 1539–1552.

[26] Y. Li, C. Tan, G.-P. Liu, Output consensus of networked multi-agent systems with time-delay compensation scheme, Journal of the Franklin Institute 353 (4) (2016) 917–935.

[27] Q. Liu, Observer-predictor feedback for consensus of discrete-time multiagent systems with both state and input delays, International Journal of Robust and Nonlinear Control 30 (10) (2020) 4003–4021.

[28] A. González, M. Aranda, G. López-Nicolás, C. Sagüés, Time delay compensation based on smith predictor in multiagent formation control, IFAC-PapersOnLine 50 (1) (2017) 11645–11651.

[29] B. Zhou, Z. Lin, Consensus of high-order multi-agent systems with large input and communication delays, Automatica 50 (2) (2014) 452–464.

[30] H. Chu, D. Yue, C. Dou, X. Xie, L. Chu, Consensus of multiagent systems with time-varying input delay via truncated predictor feedback, IEEE Transactions on Systems, Man, and Cybernetics: Systems.

[31] K. Li, C. Hua, X. You, X. Guan, Distributed output-feedback consensus control for nonlinear multiagent systems subject to unknown input delays, IEEE Transactions on Cybernetics (2020) 1–10.

[32] X. Liu, L. Dou, J. Sun, Consensus for networked multi-agent systems with unknown communication delays, Journal of the Franklin Institute 353 (16) (2016) 4176–4190.

[33] A. Ponomarev, Z. Chen, H.-T. Zhang, Discrete-time predictor feedback for consensus of multiagent systems with delays, IEEE Transactions on Automatic Control 63 (2) (2017) 498–504.

[34] Z. Wang, H. Zhang, X. Song, H. Zhang, Consensus problems for discrete-time agents with communication delay, International Journal of Control, Automation and Systems 15 (4) (2017) 1515–1523.

[35] K.-Z. Liu, X.-M. Sun, M. Krstic, Distributed predictor-based stabilization of continuous interconnected systems with input delays, Automatica 91 (2018) 69–78.

[36] W. H. Heemels, M. Donkers, A. R. Teel, Periodic event-triggered control for linear systems, IEEE Transactions on Automatic Control 58 (4) (2012) 847–861.

[37] A. Cuenca, M. Zheng, M. Tomizuka, S. Sánchez, Non-uniform multi-rate estimator based periodic event-triggered control for resource saving, Information Sciences 459 (2018) 86–102.

[38] D. Liu, G.-H. Yang, Robust event-triggered control for networked control systems, Information Sciences 459 (2018) 186–197.

[39] A. González, A. Cuenca, V. Balaguer, P. García, Event-triggered predictor-based control with gain-scheduling and extended state observer for networked control systems, Information Sciences 491 (2019) 90–108.

[40] S. Ding, X. Xie, Y. Liu, Event-triggered static/dynamic feedback control for discrete-time linear systems, Information Sciences 524 (2020) 33–45.

[41] L. Guo, H. Yu, F. Hao, Event-triggered control for stochastic networked control systems against denial-of-service attacks, Information Sciences 527 (2020) 51–69.

[42] L. El Ghaoui, F. Oustry, M. AitRami, A cone complementarity linearization algorithm for static output-feedback and related problems, IEEE Transactions on Automatic Control 42 (8) (1997) 1171–1176.

[43] Q.-L. Han, K. Gu, On robust stability of time-delay systems with norm-bounded uncertainty, IEEE Transactions on Automatic Control 46 (9) (2001) 1426–1431.

[44] C. Briat, Convergence and equivalence results for the Jensen's inequality - application to time-delay and sampled-data systems, IEEE Transactions on Automatic Control 56 (7) (2011) 1660–1665.

[45] I. R. Petersen, A stabilization algorithm for a class of uncertain linear systems, Systems & Control Letters 8 (4) (1987) 351–357.